In Proceedings of the 89th Shock and Vibration Symposium, Shock and Vibration Exchange, www.savecenter.org, Dallas, Texas, November 2018.

2D FE and 2DOF Simulations of Ground Shock Experiments – Total Structure's Spring Energy Displacement Dependency to the Charge´s and Structure´s Properties

Leo Laine[a]*, Morgan Johansson[b] and Ola Pramm Larsen[c]

[a]LL Engineering
Stugvägen 4, SE-438 94 HÄRRYDA, Sweden
*Corresponding author: leo.laine@telia.com

[b]Norconsult AB
Theres Svenssons gata 11, 417 55 GÖTEBORG, Sweden

[c]CAEwiz Consulting AS
Grinda 2B, NO-0861 OSLO, Norway

The aim for these studies is to find a methodology that can use simplified relationships for ground shock prediction, from e.g. ConWep, in combination with simplified models such as two-degree-of-freedom model (2DOF), to predict the structural response of e.g. a buried concrete wall.

This paper analyses, by using 2D axial symmetry Finite Element (FE) with Autodyn, the structural response of a well-defined structure; a suspended piston-spring system buried in sand subjected to ground shock from an explosive charge. The parameters varied in the simulations were charge size, charge distance, reflection area of the piston, piston mass, and spring stiffness. Earlier experiments from the 1980s, conducted by S. Hultgren, Swedish Fortifications, showed that the reflection pressure over time was dependent on the mass and stiffness of the structure. Here, more parameters were varied in simulations to see how well a 2DOF can capture the main behaviour of the structural response. The reflected pressure time history dependency on piston mass and spring stiffness has be confirmed by using 2DOF in earlier studies presented at SAVIAC 86, 87, and 88.

In this paper the focus is on what main parameters influence the total spring displacement energy. If the results are visualised in a 3D plot with coefficient of variation, the ratio of standard deviation and mean value, of the maximum spring energy in z-direction and the scaled charge distance and variation of piston area in x-, and y-directions, then the coefficient of variation maximum is 0.8, i.e. 80%, if one studies all results of the spring stiffness and piston mass variations. However, if the 3D plot was made for each spring stiffness 0.1 MN/m, 0.5 MN/m, and 1.2 MN/m, only study variation in mass results. This leads to that the coefficient of variation maximum drops down to 0.08, i.e. 8%, 0.025, i.e. 2.5%, and 0.03, i.e. 3.0%, respectively. This indicates that the influence of piston mass on the maximum spring energy is marginal, but the spring stiffness is important for the total spring energy during ground shock. This is also confirmed in 2D-FE simulation results where the particle velocity plots of the soil indicate that the flow of soil intensifies towards piston direction when spring stiffness value is decreased and that the moving ground shock finds the least resistant path from the detonation centre. The aim is to derive a simplified model for calculating maximum spring energy and spring displacement.

INTRODUCTION

The Swedish Civil Contingencies Agency (MSB) is responsible for the building regulations of the Swedish civil defence shelters. There are specific regulations for how the defence shelters are planned, built, equipped, and maintained [4]. One of many regulations state what load level the shelters should be able to withstand: "The effect of a pressure wave corresponding to that produced by a 250 kg GP-bomb with 50 weight percent TNT which burst freely outside at a distance of 5.0 meters from the outside of the shelter during free pressure release". However, many of the shelters are designed as basements below ground surface. Therefore, more knowledge on how the ground shock propagates and attenuates during the scaled distances of 0.1 to 10 kg/m$^{1/3}$ and effects on buried shelters, is needed.

Earlier experiments from the 1980s, conducted by S. Hultgren, Swedish Fortifications, showed that the reflection pressure over time was dependent on the mass and stiffness of the structure. The buried structure is a simple one degree of freedom (DOF) system with a piston mass and linear spring stiffness, see [1] and [2]. To increase the analysis results, simulations were conducted where more parameters were varied, such as piston area size and scaled charge distance, just to see how this influenced the structural response of the buried structure. The reflected pressure time history dependency on piston mass and spring stiffness has be confirmed by using Finite Element(FE) and 2DOF simulations in earlier studies presented at SAVIAC 86, 87, and 88, see [1], [2], and [3]. The earlier papers confirm that experimental results show the same trends as the FE-simulations. The earlier three papers also confirm that one can't use the incident pressure from ground shock and apply a reflection pressure amplification factor on the incident pressure time history and apply it on the buried structure to calculate the structural response. The reason is that the reflected pressure is dependent on the structure as mentioned earlier, see [5], [6], and [7].

Hence, to determine the pressure acting on a structure, caused by ground shock, one must also know the properties of the structure. A simplified structure, a buried suspended piston with mass m and stiffness k. Neglecting the influence of damping, the response of this structure can be described using a single degree of freedom system by using equation (1)

$$P_r(t) \cdot A = m \cdot a_x(t) + k \cdot d_x(t) \tag{1}$$

where $P_r(t)$ is the reflected pressure acting on the piston surface area A, a_x is the acceleration of the piston mass and d_x is the displacement of the piston. Fig. 1 shows the reflected pressure time history and how it contains a first mass inertia peak that increases if piston mass increases and a second spring peak which increases in amplitude if the spring stiffness increasres, this sums up the results from reports [5]-[6]. Further details about simulation results from FE and 2DOF about results of the reflected pressure, see [2], and [3].

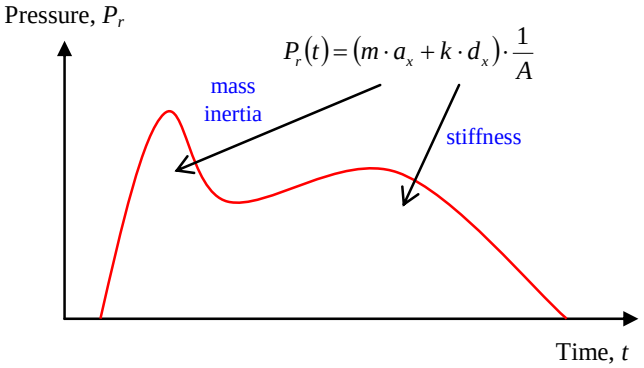

Fig. 1 Schematic illustration of how the reflection pressure $P_r(t)$ is made up of mass inertia $m \cdot a_x$ and stiffness $k \cdot d_x$ of a buried structure.

This paper uses solely simulated FE- results for the analysis. Simulations were carried out in AUTODYN-2D [8], these simulations have been earlier compared with experimental results from [5]-[6]. Total of 132 simulations have been carried out to achieve a large enough variation of parameters for the buried spring piston system, see APPENDIX I – CONDUCTED SIMULATION MATRIX.

In this paper the focus is on what main parameters influence the total spring deformation energy. The spring energy varies quite a lot for the different studied parameters, see Fig. 2. The spring energy varies from about 10 J to 13000 J.

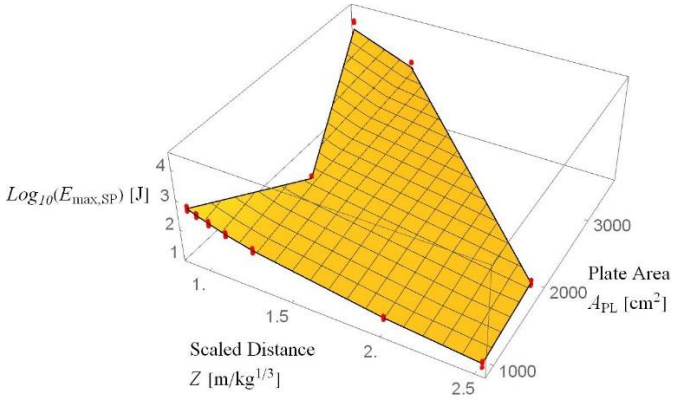

Fig. 2 3D plot of spring energy in 10 log scale as a function of scaled charge distance and piston plate area, the red dots are all spring stiffnesses and piston mass results.

To do further analysis the coefficient of variation cv will be used. The cv is calculated by dividing the standard deviation σ with the mean x_m

$$cv = \frac{\sigma}{x_m} \tag{2}$$

where standard deviation is calculated by

$$\sigma = \sqrt{\frac{\sum_{i=1}^{N}(x_i - x_m)^2}{(N-1)}} \tag{3}$$

where x_i is N observed points and x_m is the average.

The aim is to derive a simplified model for calculating maximum spring energy and spring displacement, such as 2-DOF and use simplified input from free field ground shock equations, e.g. Conwep [13]. If one studies all the spring energy results of all the spring stiffness and piston mass variations by using the coefficient of variation, the maximum is $cv = 0.8$, i.e. 80%, which is quite large, see Fig. 3. However, if the 3D plot was made for each spring stiffness 0.1 MN/m, 0.5 MN/m, and 1.2 MN/m, only study variation in mass results. This leads to that the coefficient of variation maximum drops down to 0.08, i.e. 8%, 0.025, i.e. 2.5%, and 0.03, i.e. 3.0%, respectively, see Fig. 4, Fig. 5, and Fig. 6, respectively. This indicates that the influence of piston mass on the maximum spring energy is marginal, but the spring stiffness is important for the total spring energy during ground shock. This is also confirmed in 2D-FE simulation results where the particle velocity plots of the soil indicate that the flow of soil intensifies towards piston direction when spring stiffness value is decreased and that the moving ground shock finds the least resistant path from the detonation centre, see [3]. Another observation that can be made is that the weakest spring stiffness 0.1 MN/m is the most sensitive for changing the piston plate area, see Fig. 4 and compare with Fig. 5, and Fig. 6. The stiffest spring stiffness 1.2 MN/m is more sensitive for scaled charge distance, see Fig. 6.

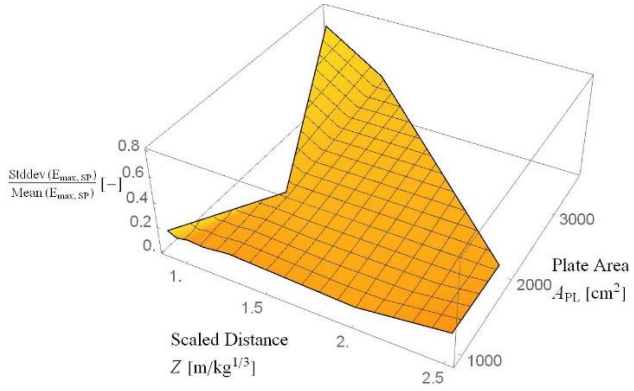

Fig. 3 3D plot of coefficient of variation for spring energy as a function of scaled charge distance and piston plate area for all spring stiffnesses and piston mass results.

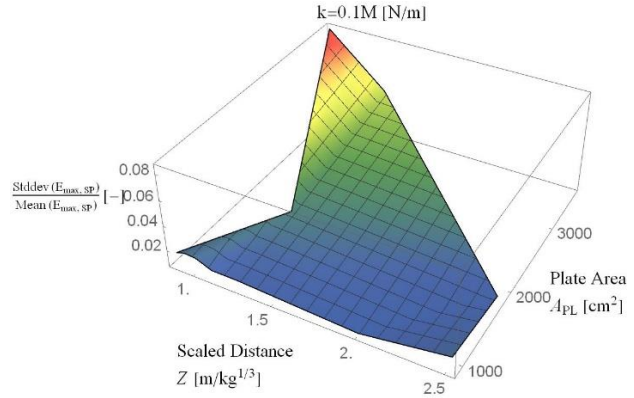

Fig. 4 3D plot of coefficient of variation for spring energy as a function of scaled charge distance and piston plate area, the spring stiffness is 0.1 MN/m and all piston mass results.

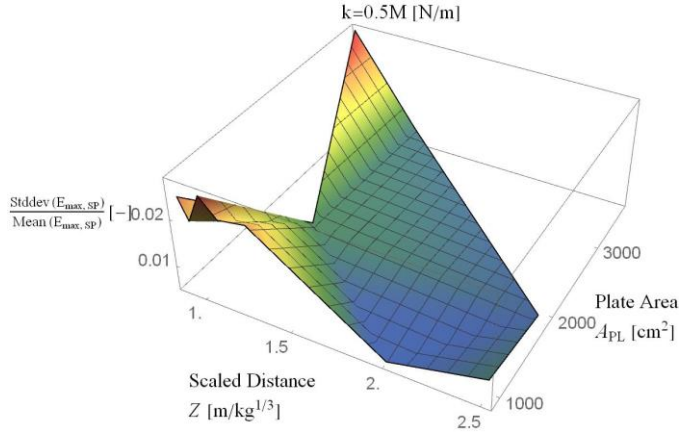

Fig. 5 3D plot of coefficient of variation for spring energy as a function of scaled charge distance and piston plate area, the spring stiffness is 0.5 MN/m and all piston mass results.

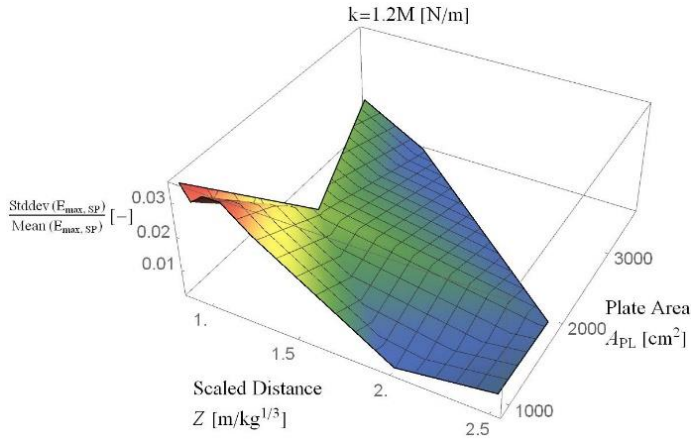

Fig. 6 3D plot of coefficient of variation for spring energy as a function of scaled charge distance and piston plate area, the spring stiffness is 1.2 MN/m and all piston mass results.

The paper is organized as follows: The section PRINCIPAL EXPERIMENTAL SETUP, describes how the simulation experiments were conducted and what parameters were varied. In section FE SIMULATION MODEL AND PARAMETERS STUDIED it is shown how the Euler and Lagrange elements were designed in AUTODYN-2D and what material models were used. In section 2DOF MODEL it is shown what parameters and initial conditions were used in the 2DOF model. In the section SIMULATION RESULTS the results from the extended parameter variation from obtained from simulations in AUTODYN-2D are analysed and compared with 2DOF. Finally, the section CONCLUSIONS AND FUTURE WORK concludes the findings from simulations and proposes suggestions for future work.

PRINCIPAL EXPERIMENTAL SETUP

The principal experimental setup is shown in Fig. 7. Both the charge of TNT with weight W kg and the suspended piston was buried d=1 m, and the distance between the charge and the piston was set to r m. The sand is modelled as dry sand [9],[10],[11], and [12], details about the simulation setup can be found in [3].

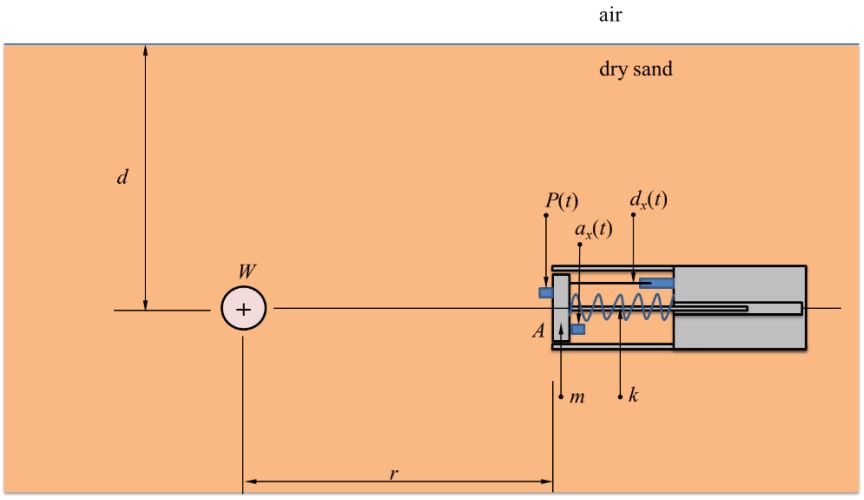

Fig. 7 Principal sketch of the experimental setup.

The main cylinder body consisted of a circular steel tube of 1.18 m in length and 0.36 m in outer diameter. The cylinder wall thickness was 8 mm and the diameter of the piston surface was 0.34 m. To increase the weight of the cylinder tube lead pieces were bolted to its inside; thus, increasing the total weight of the cylinder body to a total of 295 kg.

The piston was movable on ball bearings through an axis and the stiffness was obtained with a helical spring. The cylinder can be seen as a fixed body.

The piston's movable mass was made of a removable plate and by changing plates with different thickness the suspended mass *m* of the piston was varied [5.2, 10.6, 24.7, and 58.8 kg]. Further, by changing the helical spring the stiffness *k* was also varied [0.1, 0.5, and 1.2 MN/m]. In addition, the piston surface plate was varied.

The following measurements were installed: piston accelerometer (a_x), piston reflected pressure gauge (P_r), and relative piston displacement (d_x), see Fig. 7. Further details about the experimental setup, e.g. what model type of sensors was used, can be found in [5]. Same measurements in addition to more measurements are conducted in AUTODYN [8] models using a 2D axial symmetric geometry.

FE SIMULATION MODEL AND PARAMETERS STUDIED

The FE model was built in AUTODYN [8] using a 2D axial symmetric geometry, see Fig. 8. The TNT, sand, and void behind inside the piston was modelled with Euler cells, the piston, cylinder, and spring system was modelled with lagrange cells. The size of the model, element sizes, spring modelling, and boundaries etc. are described in [3]. The air surface part is here neglected, it means that the depth of burial is much larger than the radius, $d \gg r$, if one wants to compare to physical experiments.

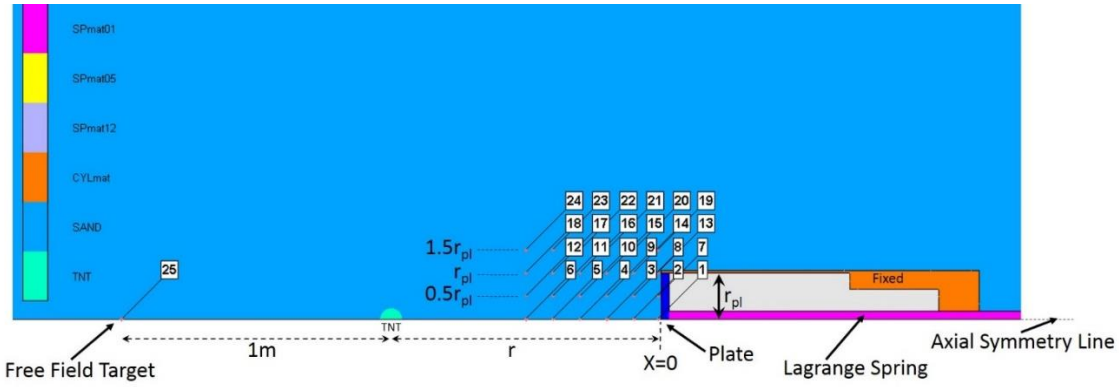

Fig. 8 2D axial symmetric model, with 25 fixed target points in the Eulerian SAND domain. The radial position of the four target rows i.e. 1-6, 7-12, 13-18, and 19-24 are located relative to the cylindrical plate (blue with radius r_{pl}). The 10m long Lagrangian spring (purple) is fixed at its right-hand side and connected to the cylindrical plate. Target 26 is located on the piston plate.

2DOF MODEL

The 2DOF model simplifies the experimental setup by the following assumptions, the sand in front of the structure is assumed to be modelled as an added mass, see Fig. 9 The explosive load is converted to either a force as function of time acting on the added mass or as a mass with an initial particle velocity on the added mass. In Fig. 10., the principal system of 2DOF is shown. The spring k_1 can only transfer compressive forces while spring k_2 can transfer forces in both directions. The initial velocity v_0 (i.e. the sand particle velocity U_{p0}) is used for describing the movement of the sand generated by the explosion. The depth of burial is seen as

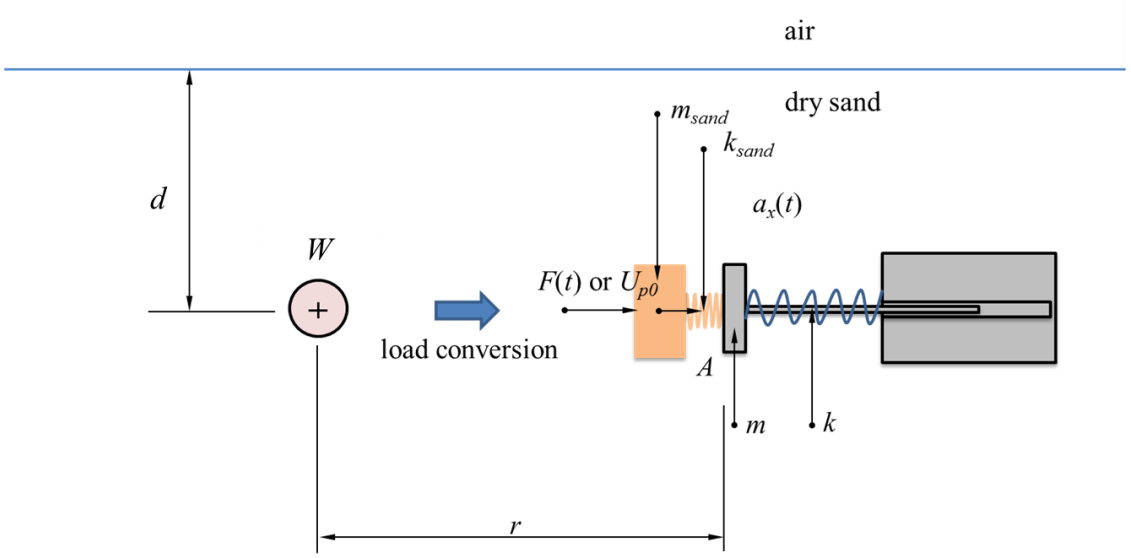

Fig. 9 *Illustration of how the 2DOF model is set up. The piston mass is connected to a second mass which is assumed to be an added mass from the sand and during compression the masses have a spring stiffness based on the bulk modulus of the sand.*

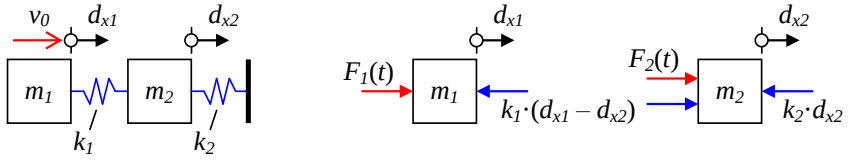

Fig. 10 *Illustration of 2DOF model used. Spring k_1 can only transfer compressive forces while spring k_2 can transfer forces in both directions.*

The equations used to solve the 2DOF model can be written as

$$\begin{bmatrix} m_1 & 0 \\ 0 & m_2 \end{bmatrix} \begin{bmatrix} a_{x1} \\ a_{x2} \end{bmatrix} + \begin{bmatrix} k_1 & -k_1 \\ -k_1 & k_1 + k_2 \end{bmatrix} \begin{bmatrix} d_{x1} \\ d_{x2} \end{bmatrix} = \begin{bmatrix} F_1(t) \\ 0 \end{bmatrix} \tag{4}$$

where m_1 and m_2 is the sand mass and mass of the piston plate, respectively, k_1 is the stiffness of the sand cone and k_2 is the stiffness of the spring. Further $\ddot{u}_1$ and $\ddot{u}_2$ are accelerations and u_1 and u_2 are displacements of masses m_1 and m_2, respectively. To correctly simulate that sand cannot transfer tensile forces the sand spring k_1 was modified so that only compressive forces could be transferred; spring k_2 though was linear elastic in both directions. The influence of damping was assumed to be negligible and is hence not included in the model. The added mass of sand is calculated as the mass of a cone between the charge point and the piston plate (i.e. the base of the cone) as

$$m_{sand} = A \cdot \frac{r}{3} \cdot \rho_{sand} \tag{5}$$

where A is the area of the piston plate, r is the charge distance and ρ_{sand} = 1674 kg/m^3 is the sand in situ density.

The linear spring stiffness of the sand is approximated as

$$k_{sand} = \frac{K_{sand} \cdot A}{l_{cone}} \tag{6}$$

where K_{sand} is the sand bulk modulus and

$$l_{cone} = \frac{r}{3} \tag{7}$$

is the distance from the centre point of the sand cone to the piston plate. The bulk modulus was approximated to be equal both for loading and unloading cases and was determined as

$$K_{sand} = \rho_{sand} \cdot c_{sand}^{\ 2} \tag{8}$$

where c_{sand} = 350 m/s is the speed of the pressure wave (a typical value for dry soil [12]). This gives a sand bulk modulus of K_{sand} = 0.2 GPa (as a comparison, this is about ten times smaller than the bulk modulus of water, $K_{water} = 1000 \cdot 1484^2$ = 2.2 GPa). The model parameters for all cases are gathered in Table 1.

Table 1 Model parameters used in the 2DOF model for the cases studied.

Identification		Part 1: Sand		Part 2: Spring	
Group	Case	m_{sand} [kg]	k_{sand} [MN/m]	m [kg]	k [MN/m]
1	1-12	50.7	56	5.2 – 58.8	0.1 – 1.2
2	13-24	101.3	112	5.2 – 58.8	0.1 – 1.2
3	25-36	202.6	223	5.2 – 58.8	0.1 – 1.2
4	37-48	50.7	56	5.2 – 58.8	0.1 – 1.2
5	49-60	50.7	56	5.2 – 58.8	0.1 – 1.2
6	61-72	50.7	56	5.2 – 58.8	0.1 – 1.2
7	73-84	50.7	56	5.2 – 58.8	0.1 – 1.2
8	85-96	101.3	28	5.2 – 58.8	0.1 – 1.2
9	97-108	202.6	223	5.2 – 58.8	0.1 – 1.2
10	109-120	101.3	28	5.2 – 58.8	0.1 – 1.2
11	121-132	202.6	56	5.2 – 58.8	0.1 – 1.2

In previous work, see [1] and [2], the initial particle velocity used was derived with ConWep [13] for a sand with 1674 kg/m^3 in density, seismic wave speed 350 m/s, and 2.75 attenuation factor. This gave a particle velocity of 1.5 m/s for the selected charge size and distance to target (0.5 kg and 1.0 m respectively). In [3], the particle velocities from Autodyn simulations have been used instead.

SIMULATION RESULTS

Simulations were carried out for a total of 12 combinations of different piston mass [5.2, 10.6, 24.7, 58.8 kg] and spring stiffness [0.1, 0.5, 1.2 MN/m]. For each of these combinations, the charge size W [0.5, 0.75, 1.0, 1.5 kg TNT] and the horizontal distance r, between charge and piston plate, was in one case also varied [1, 2 m]. Further, for some groups the piston contact surface was increased in size: $\Delta A = (A\text{-}A_0)/A_0 \cdot 100$, [0, 100, 300 %]. A total of 11 groups, each with 12 simulations, were conducted; resulting in a total number of 132 simulations, see Table 2 and

APPENDIX I – CONDUCTED SIMULATION MATRIX.

Table 2 Summary of simulations carried out. In each group the piston mass [5.2, 10.6, 24.7, 58.8 kg] and spring stiffness [0.1, 0.5, 1.2 MN/m] were varied, resulting in a total of 132 simulations.

Group	Case	W [kg]	r [m]	ΔA [%]
1	1-12	0.50	1.0	0
2	13-24	0.50	1.0	100
3	25-36	0.50	1.0	300
4	37-48	0.75	1.0	0
5	49-60	1.00	1.0	0
6	61-72	1.25	1.0	0
7	73-84	1.50	1.0	0
8	85-96	0.50	2.0	0
9	97-108	1.50	1.0	300
10	109-121	1.00	2.0	0
11	121-132	0.50	2.0	100

In section INTRODUCTION, it was shown by studying the coefficient of variation for spring displacement energy that the maximum spring energy is independent of the piston mass. The spring energy can be determined as the internal work made by the spring and can be calculated as

$$W_i = \frac{k \cdot d_{x,\max}^2}{2} \tag{9}$$

where k is the spring stiffness and $d_{x,max}$ is the maximum displacement of the spring.

In Table 3, the average and standard deviation spring energy for the different spring stiffnesses are shown. The largest spring energy is obtained in simulation group 9 (scaled charge distance 0.87 m/kg$^{1/3}$, spring plate area 300% larger than smallest value and spring stiffness 0.1 MN/m) where a value of 12560 J is reached. In the same simulation group 9, the maximum spring energy reduces to 4180 J and 3213 J, when spring stiffness is increased to 0.5 MN/m and 1.2 MN/m, respectively, see Table 3. This clearly indicates the leakage effect of a closed in explosion. When the scaled distance is kept constant and the smallest spring plate area is used, simulation group 7, the maximum spring energies reduce to 592 J, 475 J, and 409 J for spring stiffness 0.1 MN/m, 0.5 MN/m, and 1.2 MN/m, respectively. This means that the maximum spring energy increases 21 times for spring stiffness 0.1 MN/N when the piston plate area is increased with 300 % for scaled charge distance 0.87 m/kg$^{1/3}$. It increases more moderately for the stiffer springs, 9 and 8 times for spring stiffness 0.5 MN/m and 1.2 MN/m. Comparing simulation group 3 and group 1 where the scaled charge distance is kept constant at 1.26 m/kg$^{1/3}$ but the spring plate area is increased 300 % in group 3. There the increase is 10, 8, and 7 times increase in spring energy for spring stiffnesses 0.1 MN/m, 0.5 MN/m, and 1.2 MN/m, respectively, see group 3 and group 1 in Table 3.

Table 3 Summary of results for maximum spring displacement energy from Autodyn simulations. In each group spring stiffness [0.1, 0.5, 1.2 MN/m] were varied and mean value and standard deviation are given for all the piston masses [5.2, 10.6, 24.7, 58.8 kg].

Simulation group	Spring stiffness	Scaled charge distance	Piston plate area increase	Maximum spring energy		
Group	k [MN/m]	R [m/kg$^{1/3}$]	$(A\text{-}A_0) / A_0 \cdot 100$ [%]	$W_{i,m}$ [J]	σ_W [J]	$\sigma_W / W_{i,m}$ [%]
1	0.1	1.26	0	139	1.6	1.2
	0.5			111	2.3	2.0
	1.2			97	2.3	2.4
2	0.1	1.26	100	400	8.1	2.0
	0.5			311	3.0	1.0
	1.2			258	3.7	1.4
3	0.1	1.26	300	1512	60.7	4.0
	0.5			876	7.1	0.8
	1.2			680	1.7	0.2
4	0.1	1.1	0	219	2.6	1.2
	0.5			184	3.6	1.9
	1.2			160	4.7	2.9
5	0.1	1	0	328	5.4	1.6
	0.5			274	6.2	2.3
	1.2			235	6.8	2.9
6	0.1	0.93	0	431	7.3	1.7
	0.5			366	6.4	1.7
	1.2			321	8.6	2.7
7	0.1	0.87	0	592	9.1	1.5
	0.5			475	10.0	2.1
	1.2			409	12.5	3.0
8	0.1	2.52	0	16.3	0.26	1.6
	0.5			18.3	0.16	0.9
	1.2			11.2	0.07	0.6
9	0.1	0.87	300	12560	935	7.4
	0.5			4180	102	2.4
	1.2			3213	38.0	1.2
10	0.1	2	0	32.3	0.24	0.7
	0.5			28.1	0.13	0.5
	1.2			24.5	0.07	0.3
11	0.1	2.52	100	29.8	0.33	1.1
	0.5			39.2	0.27	0.7
	1.2			25.2	0.14	0.6

The spring energy as a function of time is shown in Fig. 11 and Fig. 12 for groups 1 and 3 and groups 7 and 9, respectively. It is clear that the piston mass does not influence the maximum spring energy.

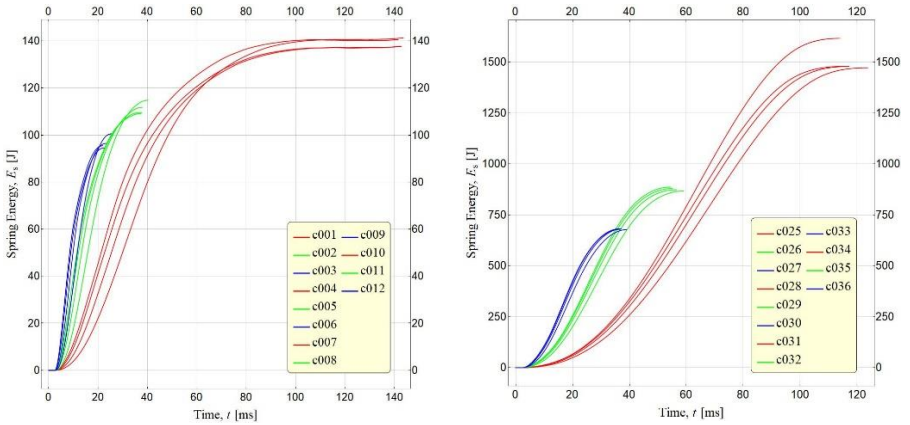

(1a) (1b)

Fig. 11 Spring energy as a function of time for simulation group 1 (1a) and for simulation group 3 (1b). The scaled charge distance is 1.26 m/kg$^{1/3}$ and piston plate area is increased 300% in group 3.

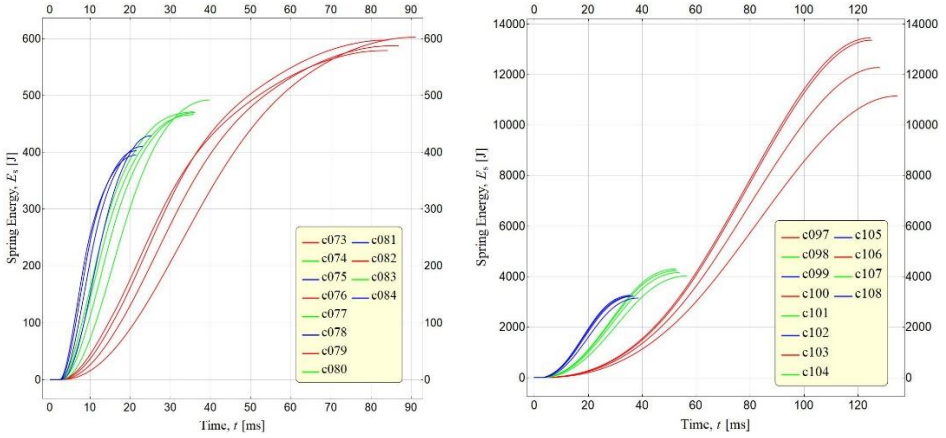

(1a) (1b)

Fig. 12 Spring energy as a function of time for simulation group 7 (1a) and for simulation group 9 (1b). The scaled charge distance is 0.87 m/kg$^{1/3}$ and piston plate area is increased 300% in group 3.

There is a way to normalise the particle velocity for different radius distances from charge by studying the flux, the flow rate per unit area for an incompressible material. The flow rate per area shall remain the same for an incompressible material. This means that the spreading sphere surface area times the particle velocity at that radius shall remain equal. Following equation is used for normalising the particle velocities and piston velocity:

$$4 \cdot \pi \cdot r_1^2 \cdot u_{p1} = 4 \cdot \pi \cdot r_i^2 \cdot u_{pi} \tag{10}$$

Where r_1 and u_{p1} are radius and particle velocity at target point 1, see Fig. 8.

This gives following normalized particle and piston velocities for one simulation in group 1 and group 3, see Fig. 13 and Fig. 14. The free field particle velocities compare well with solid lines before the time ground shock wave reach the piston. Then it can be observed that the particle velocity and piston velocity increase about 70 percent when studying the spherically normalized particle velocity, see left plot (1a) in Fig. 13. Comparing right plots (1b) in Fig. 13 and Fig. 14 shows that when the piston plate increases with 300% there is a significant increase in the normalized particle velocities in the sand. This is a clear indication of vent leakage for a closed in explosion. In Fig. 14 (1b) measurement point #6 is cut at 50 ms, due to that the TNT gas expansion has reach this measurement point which gives high oscillations in measurement of particle velocity.

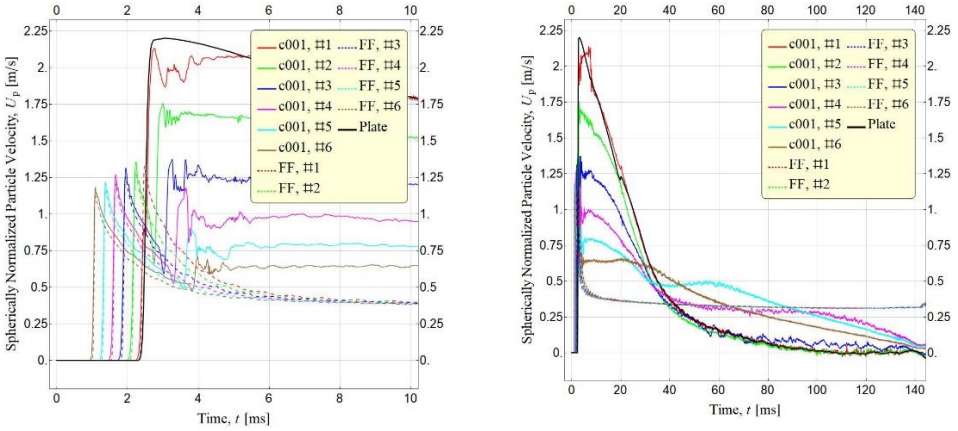

(1a) (1b)

Fig. 13 Spherically normalised particle velocity and piston velocity as a function of time for simulation group 1 with stiffness 0.1 MN/m and piston mass 5.2 kg and free field dashed lines. First 5 ms (1a) and results until piston reaches zero velocity (1b). The scaled charge distance is 1.26 m/kg$^{1/3}$ and piston plate area is original.

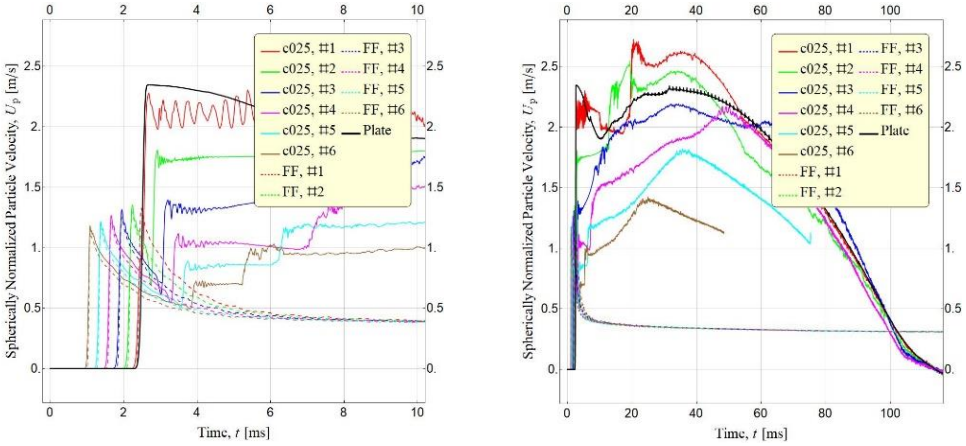

(1a) (1b)

Fig. 14 Spherically normalised particle velocity and piston velocity as a function of time for simulation group 3 with stiffness 0.1 MN/m and piston mass 5.2 kg and free field dashed lines. First 10 ms (1a) and results until piston reaches zero velocity (1b). The scaled charge distance is 1.26 m/kg$^{1/3}$ and piston plate area is increased 300% in group 3.

This gives following normalized particle and piston velocities for one simulation in group 7 and group 9, see Fig. 15 and Fig. 16. The free field particle velocities compare well with solid lines before the time ground shock wave reach the piston. Then it can be observed that the particle velocity and piston velocity increase about 60 percent when studying the spherically normalized particle velocity, see left plot (1a) in Fig. 15. Comparing right plots (1b) in Fig. 15 and Fig. 16. shows that when the piston plate increases with 300% there is a significant increase in the normalized particle velocities in the sand. This is a clear indication of vent leakage for a closed in explosion. In Fig. 15 (1b) measurement point #6 is cut at 40 ms, due to that the TNT gas expansion has reach this measurement point which gives high oscillations in the particle velocity. In Fig. 16 (1b) measurement points #1-#6 are cut between 20-100 ms, due to that the TNT gas expansion has reach this measurement point which gives high oscillations in the measurement of particle velocity.

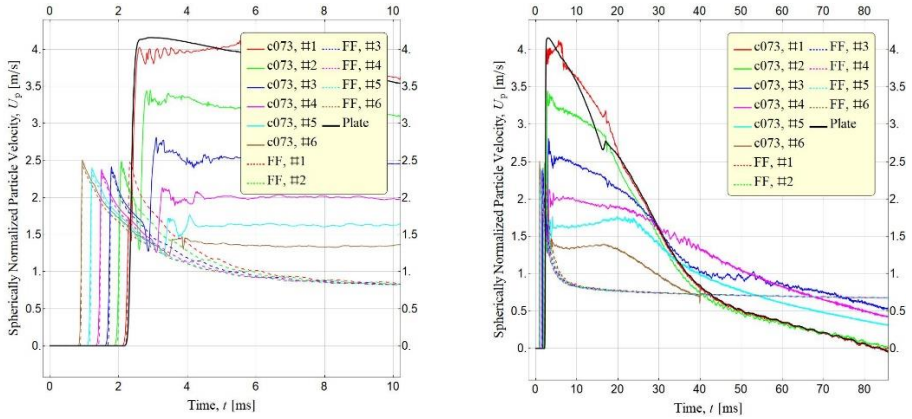

(1a) (1b)

Fig. 15 Spherically normalised particle velocity and piston velocity as a function of time for simulation group 7 with stiffness 0.1 MN/m and piston mass 5.2 kg and free field dashed lines. First 10 ms (1a) and results until piston reaches zero velocity (1b). The scaled charge distance is 0.87 m/kg$^{1/3}$ and piston plate area is original.

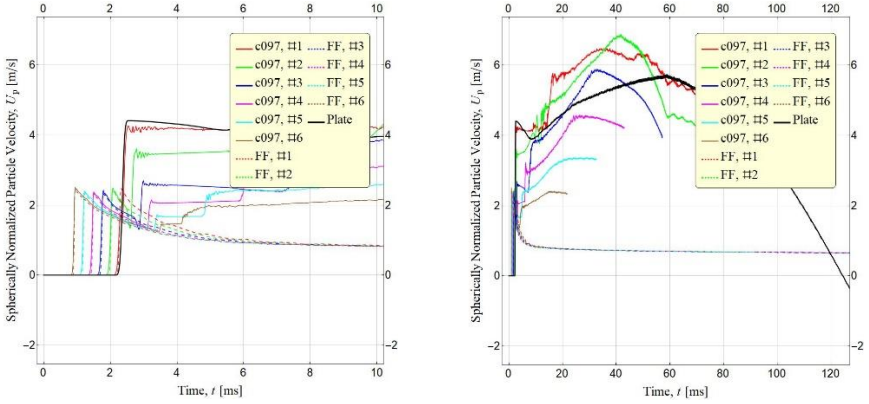

(1a) (1b)

Fig. 16 Spherically normalised particle velocity and piston velocity as a function of time for simulation group 9 with stiffness 0.1 MN/m and piston mass 5.2 kg and free field dashed lines. First 10 ms (1a) and results until piston reaches zero velocity (1b). The scaled charge distance is 0.87 m/kg$^{1/3}$ and piston plate area is increased 300% in group 9.

By studying the TNT gas development for group 9 which has the largest leakage energy it can be observed that the TNT gas sphere becomes highly un-symmetric after a while, Fig. 17. At 120 ms, see Fig. 17., right plot (1b), shows that the gas bubble has reached the opening of the cylinder. This phenomenon, with energy valve leakage, is hard to simulate with just added sand mass with and with a combination of long-term external pressure when using a 2-DOF like model.

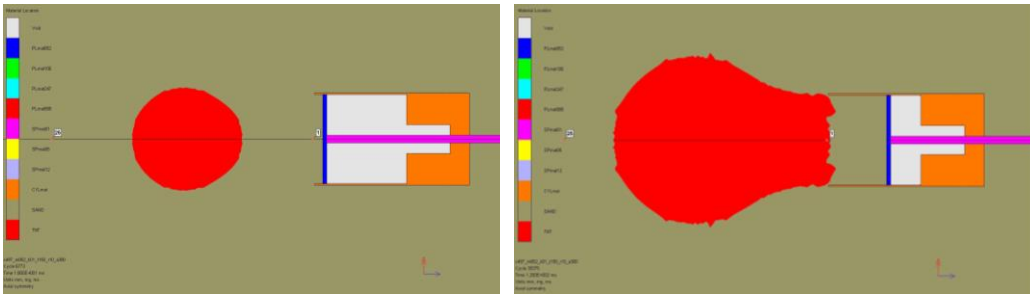

(1a) (1b)

Fig. 17 TNT gas bubble in sand simulation group 9 with stiffness 0.1 MN/m and piston mass 5.2 kg. Material location at 18 ms (1a) and and material localisation at 120 ms (1b). The scaled charge distance is 0.87 m/kg$^{1/3}$ and piston plate area is increased 300% in group 9.

COMPARISON WITH 2DOF MODEL

A simplified 2DOF model is used to compare the results obtained in using Autodyn. In this comparison the external work is assumed to be equal to the kinetic energy of the sand and piston shortly after the initial acceleration of the piston. At this moment the particle velocity of the sand in front of the piston plate and the piston plate is about the same. From this the external work of the system has been approximately determined as

$$W_y = E_k = \frac{\left(m_{sand} + m\right) \cdot v_o^{\,2}}{2} \tag{11}$$

where m_{sand} and m are the mass of the sand cone (equation (5)) and the piston mass, and v_o is the maximum initial velocity of the piston. Hence, this approximation assumes that a plastic impact between the sand cone and the piston plate has taken place and that no other external force is applied on the spring after that. If this is true, the external work will be equal to the maximum spring energy; i.e. $W_y = W_i$. However, in Fig. 18 it is shown that this simple relation is not correct. For some load cases the ratio $W_i / W_y \approx 1.0$ but in several cases this ratio differs rather much. Hence, an additional parameter, here denoted as W_{leak}, is introduced defined as

$$W_{leak} = W_i - W_y \tag{12}$$

This part thus corresponds to the extra external energy amount that has to be applied to the piston to get an energy balance between internal work W_i (spring energy) and the external work ($W_y + W_{leak}$) and the ratio W_{leak} / W_y is presented in Fig. 18.

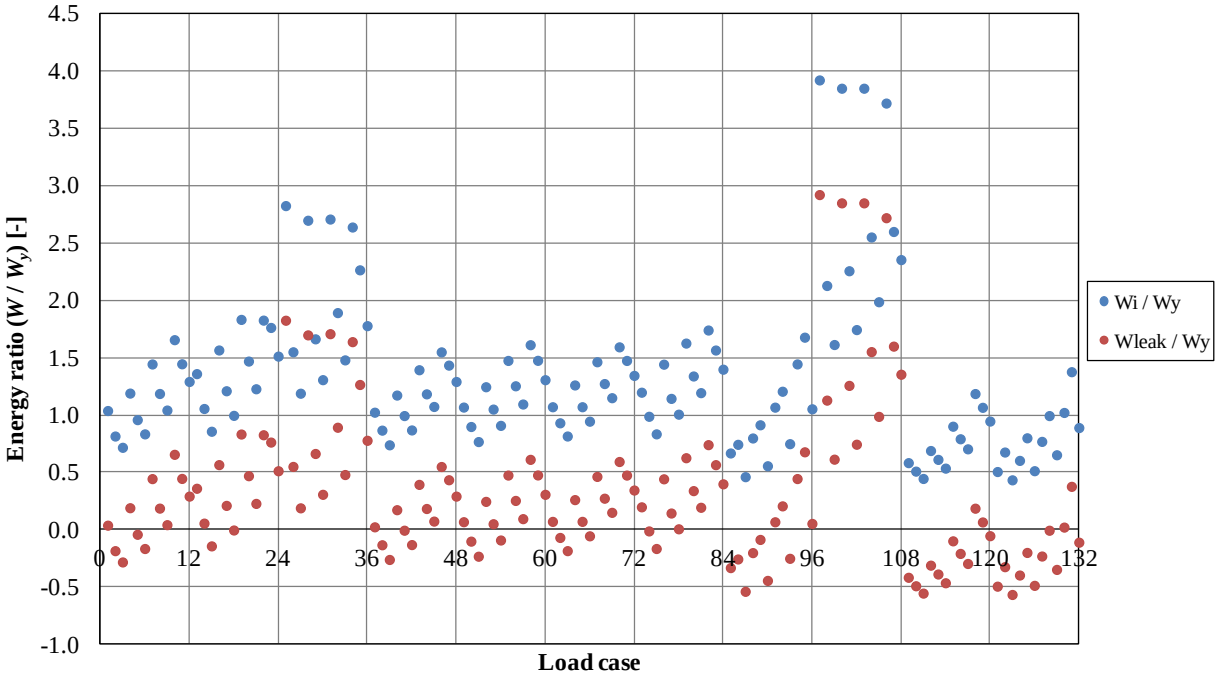

Fig. 18 Summary of energy ratios W_i / W_y and W_{leak} / W_y for the studied load cases.

In Table 3 it is shown that the influence of mass on the maximum spring energy is negligible. The same conclusion, though, cannot be made based on Fig. 18; instead, there is a clear influence here that there is an influence of the piston mass. Consequently, the simplified approximation made in equation (11) is not enough to represent what happens in the Autodyn simulations. There is a need for an additional factor that influence the total external work applied on the spring.

From Fig. 18 it can also be concluded that the energy ratio W_i / $W_y \approx 0.7 – 1.7$ when r = 1.0 m and ΔA = 0 % (group 1, 4-7); i.e. a similar relation is obtained regardless of charge weight W. For a larger charge distance, r = 2.0 m (group 8, 10, 11) this ratio is lower, W_i / $W_y \approx 0.4 – 1.4$, with most cases overestimating the value of W_y; i.e. $W_{leak} < 0$, meaning that the sand mass m_{sand} used in equation (11) is too high. The largest deviations are obtained when ΔA = 300 % (group 3, 9); especially when the spring stiffness is small (0,1 MN/m). This indicates that the additional external work applied on the piston is related to both the plate area and the spring stiffness. Both these parameters can also be related to an extra external force acting on the piston during the duration of the spring displacement.

CONCLUSIONS AND FUTURE WORK

2D Finite Element simulations have been carried out in Autodyn to study the structural response of a well-defined structure; a suspended piston-spring system buried in sand subjected to ground shock from an explosive charge. The parameters varied in the simulations were charge size, charge distance, reflection area of the piston, piston mass, and spring stiffness; a total of 132 load cases were studied. Further attempts have been made to approximately describe the structural response using a simplified 2DOF model; describing the sand and structure, respectively.

So far following main conclusions can be made. Firstly, when studying variation of coefficient for the maximum spring energy, the results are independent of the mass. This means that spring energy increases only due to a weaker spring stiffness and don't vary with piston mass. Secondly, a weaker spring leads to larger particle velocity in the sand near the piston when particle and piston velocity is flux normalised as for incompressible materials for different spherical radius. This means that large piston area and weak spring performs like leakage valve for a closed in explosion. Thus, the spring energy is increased if the spring is weak and piston area is large. Thirdly, the 2-DOF model

approach needs further development to explain the phenomena described in first and second conclusion. The kinetic energy from added mass from sand hitting the piston with a certain initial velocity is not enough. Another, not so appealing approach is to limit the usage of 2-DOF model when too weak structures are analysed.

Further studies will be made to examine if the simplified approach with 2-DOF or similar method can account for the physics of the weak spring leakage phenomena which increases the maximum spring energy.

ACKNOWLEDGEMENTS

The authors acknowledge the support given by MSB and especially Lars Gråbergs. Additionally, members of the West Coast Sweden Shock Wave Group (WCSSWG), and especially Dr. Joosef Leppänen, are highly acknowledged for their input.

REFERENCES

[1] Laine, L., Johansson, M., and Larsen O.P. (2015): "Simulation of experiments which show that reflection pressure time history from ground shock depends on the reflected structure's stiffness and mass", *Proceedings of the 86th Shock and Vibration Symposium*, Orlando, FL, USA.

[2] Laine, L., Johansson, M., and Larsen O.P. (2016): "3D FE and 2DOF simulations of ground shock experiments – Reflection pressure time history dependency due to the structure's stiffness and mass", *Proceedings of the 87th Shock and Vibration Symposium*, New Orleans, LA, USA.

[3] Laine, L., Johansson, M., and Larsen O.P. (2017): "2D FE and 2DOF Simulations of Ground Shock Experiments – Reflection Pressure Time History Dependency due to the Charge´s and Structure´s Properties", *Proceedings of the 88th Shock and Vibration Symposium*, Jacksonville, Florida, USA.

[4] Ekengren B. (2018): *Skyddsrum, SR 15* (Civil Defence Shelters SR 15, in Swedish.), the Swedish Civil Contingencies Agency (MSB), report no. MSB748, ISBN 978-91-7383-485-8, Karlstad, Sweden.

[5] Hultgren S. (1979): *Explosion of buried model structures to buried TNT explosions in sand*, Fortfikationsförvaltningen Fortf, Report nr C 183, Eskilstuna, Sweden.

[6] Hultgren S. (1980): (*Effect of underground explosions in the sand with deformable walls, in Swedish*), Omgång II, Fortfikationsförvaltningen Fortf, Rapport nr C 200, Eskilstuna, Sweden.

[7] Hultgren S. (1985): *On the effects of buried explosions in sand*, Fortfikationsförvaltningen Fortf, Report nr C2:85, Eskilstuna, Sweden.

[8] Century Dynamics Inc. (2004*): AUTODYN Theory Manual Revision 5.0*, San Ramon, CA, USA.

[9] Laine L. and Sandvik A. (2001): "Derivation of mechanical properties for sand", 4th Asian-Pacific conference on **Shock** and Impact Loads on Structures, CI-Premier PTE LTD, vol. 4, pp 353-360, Singapore.

[10] Heyerdahl H. and Madshus C. (2000): "EOS-data for sand, Tri-axial tests on sand from Sjöbo", Norges Geotekniske institutt, NGI rept. 20001157-1, Oslo, Norway.

[11] Laine L. and Larsen O.P. (2012): "Implementation of Equation of State for Dry Sand in Autodyn", *83rd Shock and Vibration Symposium, Shock and Vibration Exchange (SAVE)*, New Orleans, LA.

[12] Laine L. (2012): *Markstötvåg* (Ground Shock. In Swedish). MSB, Myndigheten för samhällsskydd och beredskap. Publ.nr MSB344, Karlstad.
Weblink:https://www.msb.se/Upload/Insats_och_beredskap/Olycka_kris/Skyddsrum/Litteratur/L01.%20Referenslitteratur/L01-202_Markst%C3%B6tv%C3%A5g.pdf

[13] ConWep (1992): Collection of conventional weapons effects calculations based on TM 5-855-1, Fundamentals of Protective Design for Conventional Weapons, U.S. Army Engineer Waterways Experiment Station, Vicksburg, USA.

APPENDIX I – CONDUCTED SIMULATION MATRIX

	Buried Plate-Spring System 2D Autodyn Simulations 2018						
		Structure		Charge and Distance		Scaled charge distance	Plate Area Increase
Sim ID	Group	m [kg]	k_0 [MN/m]	m_{TNT} [kg]	r [m]	R [m/kg$^{1/3}$]	$(A-A_0)/A0*100$ [%]
c001	1	5.2	0.1	0.5	1	1.26	0
c002			0.5				
c003			1.2				
c004		10.6	0.1				
c005			0.5				
c006			1.2				
c007		24.7	0.1				
c008			0.5				
c009			1.2				
c010		58.8	0.1				
c011			0.5				
c012			1.2				
c013	2	5.2	0.1	0.5	1	1.26	100
c014			0.5				
c015			1.2				
c016		10.6	0.1				
c017			0.5				
c018			1.2				
c019		24.7	0.1				
c020			0.5				
c021			1.2				
c022		58.8	0.1				
c023			0.5				
c024			1.2				
c025	3	5.2	0.1	0.5	1	1.26	300
c026			0.5				
c027			1.2				
c028		10.6	0.1				
c029			0.5				
c030			1.2				
c031		24.7	0.1				
c032			0.5				
c033			1.2				
c034		58.8	0.1				
c035			0.5				
c036			1.2				
c037	4	5.2	0.1	0.75	1	1.10	0

c038			0.5				
c039			1.2				
c040		10.6	0.1				
c041			0.5				
c042			1.2				
c043		24.7	0.1				
c044			0.5				
c045			1.2				
c046		58.8	0.1				
c047			0.5				
c048			1.2				
c049	5	5.2	0.1	1	1	1	0
c050			0.5				
c051			1.2				
c052		10.6	0.1				
c053			0.5				
c054			1.2				
c055		24.7	0.1				
c056			0.5				
c057			1.2				
c058		58.8	0.1				
c059			0.5				
c060			1.2				
c061	6	5.2	0.1	1.25	1	0.93	0
c062			0.5				
c063			1.2				
c064		10.6	0.1				
c065			0.5				
c066			1.2				
c067		24.7	0.1				
c068			0.5				
c069			1.2				
c070		58.8	0.1				
c071			0.5				
c072			1.2				
c073	7	5.2	0.1	1.5	1	0.87	0
c074			0.5				
c075			1.2				
c076		10.6	0.1				
c077			0.5				
c078			1.2				
c079		24.7	0.1				
c080			0.5				

c081			1.2				
c082		58.8	0.1				
c083			0.5				
c084			1.2				
c085	8	5.2	0.1	0.5	2	2.52	0
c086			0.5				
c087			1.2				
c088		10.6	0.1				
c089			0.5				
c090			1.2				
c091		24.7	0.1				
c092			0.5				
c093			1.2				
c094		58.8	0.1				
c095			0.5				
c096			1.2				
c097	9	5.2	0.1	1.5	1	0.87	300
c098			0.5				
c099			1.2				
c100		10.6	0.1				
c101			0.5				
c102			1.2				
c103		24.7	0.1				
c104			0.5				
c105			1.2				
c106		58.8	0.1				
c107			0.5				
c108			1.2				
c109	10	5.2	0.1	1	2	2	0
c110			0.5				
c111			1.2				
c112		10.6	0.1				
c113			0.5				
c114			1.2				
c115		24.7	0.1				
c116			0.5				
c117			1.2				
c118		58.8	0.1				
c119			0.5				
c120			1.2				
c121	11	5.2	0.1	0.5	2	2.52	100
c122			0.5				
c123			1.2				

c124		10.6	0.1				
c125			0.5				
c126			1.2				
c127		24.7	0.1				
c128			0.5				
c129			1.2				
c130		58.8	0.1				
c131			0.5				
c132			1.2				